# Numerical model updating of an aging steel bridge based on a multidisciplinary experimental campaign

**Brais Barros, Borja Conde, Óscar Bouzas, Manuel Cabaleiro, Belén Riveiro**

Universidad de Vigo, CINTECX-Universidade de Vigo-GeoTECH Group, Vigo, Spain.

**Contact:** brais.barros.gonzalez@uvigo.es

## Abstract

A large part of the European bridge stock is reaching the end of its design service life. Currently, several applications for numerical models have been emerged, such as damage detection or structural safety assessment, among others. However, accurate numerical modeling is still a challenge. Model input uncertainties can cause large differences between numerical model predictions and actual measured responses from the structure. This fact makes model updating or calibration techniques essential for the aim of reducing such discrepancies. In this study, a model updating methodology is developed and implemented in an aging steel bridge located in a corrosive environment. An extensive and multidisciplinary experimental campaign was first carried out for collecting the necessary geometrical and material properties as well as dynamic data that will be used as a reference for the calibration process. A good agreement was found between the updated numerical model and the experimental modal data obtaining an average frequency error of 2.09% and average MAC (Modal Assurance Criterion) of 0.97.

**Keywords:** Model updating, Sensitivity analysis, Multidisciplinary experimental campaign, Aging steel bridge.

## 1 Introduction

Within the transportation network, bridges are one of the most important assets. In the European framework, a great number of bridges currently overpass their expected lifetime or are very close to. Moreover, many of them are subjected to heavy traffics loads and are located in areas where the salinity, humidity, and highs winds cause significant corrosion effects. For these reasons, bridge maintenance has turned into a critical task.

The development of numerical models is a very useful tool to assess the current state of a structure, investigate causes of damage, or perform robustness analysis. Ancient structures require obtaining a significant amount of data to perform accurate numerical modeling. For this reason, the deployment of extensive experimental campaigns is usually needed, targeted to an accurate geometrical characterization and/or to the reduction of uncertainties in material properties or connections' stiffness, among others.

Numerical model updating is a procedure that allows approximating simulation outcomes to the real observed mechanical behavior of the bridge. For this purpose, operational modal analysis is commonly adopted to obtain the modal properties (natural frequencies, mode shapes, and damping ratios) that enable characterizing the overall system response. These data can then be employed as "ground truth" in the calibration process. In this work, a deterministic approach is adopted to perform the Finite Element (FE)

model updating of a historical steel arch bridge supported by experimental data obtained in a multidisciplinary campaign. Aimed at reducing the computational cost of the calibration process, a sensitivity analysis is first performed. Subsequently, the optimization stage is carried out by means of a nonlinear least-squares algorithm. Finally, the frequency errors and the MAC (Modal Assurance Criterion) values obtained are compared between the initial and the updated numerical model.

## 2 Case study

The bridge considered in this study is located in the Sor river, between the municipalities of Mañon (O Barqueiro) and Vicedo, in the north region of Galicia, Spain. It was built in 1901 and is made of laminated steel plates and L-shaped profiles assembled through riveted connections. It has a total length of 150 m and is placed in a maritime zone characterized by a high degree of salinity in the environment and strong winds. These factors cause elevate corrosion and deterioration in the structure. The bridge was restored in 2006 and nowadays has turned into a footbridge.

The bridge has three isostatic spans. The span analyzed here (the first from the right in Figure 1) has a length of 48,10 m, a width of 6,40 m, and a height of 7.50 m. The deck is composed of 65 stringers and 14 transverse beams of an I-shaped profile. The steel members that built up the arch and the external longitudinal girder present an H-shaped cross-section. They are linked to the deck by means of 24 pairs of T-shaped hangers which are in turn assembled by utilizing several lacings. Moreover, the bridge is vertically and laterally stiffened by 34 lateral bracings and 44 cross bracings.

*Figure 1. Upstream view of O Barqueiro bridge.*

## 3 Experimental campaign

A multidisciplinary experimental campaign was carried out to obtain a sufficient amount of data to build an accurate numerical model. The different stages of the experimental campaign were: visual inspection and on-site measurements, three-dimensional geometrical characterization through terrestrial laser scanning, and dynamic identification through Operational Modal Analysis (OMA).

### 3.1 Visual inspection and on-site measurements

As the first stage, a visual inspection was carried out to determine the condition state of all bridge elements, and especially for having a depth insight into the severity and corrosion extension in the different steel plates. Despite the restoration works performed in 2006, the bridge currently presents a high degree of corrosion. Indeed, the most damaged elements are the repaired hangers. Figure 2 details the lack of material and existing rust in the lower part of two of the hangers.

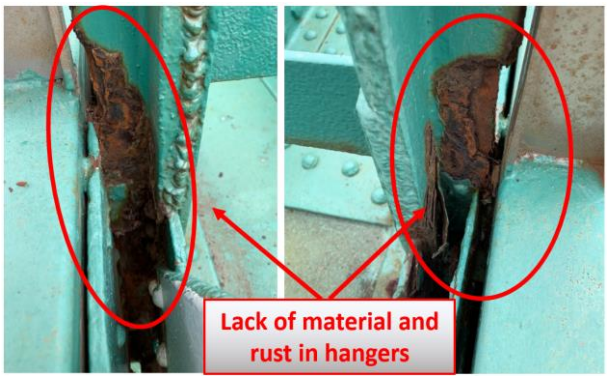


*Figure 2. Example of damaged hangers.*

Thus, to detail its corrosion status, all connections have been individually inspected and qualitatively classified according to their damage condition. This classification was mainly based on engineering judgment, considering several criteria, among others if there were superficial or pitted corrosion, lack of rivets, or the detachment of the steel plates. The damage state of each connection is schematically depicted in the mapping of Figure 3.

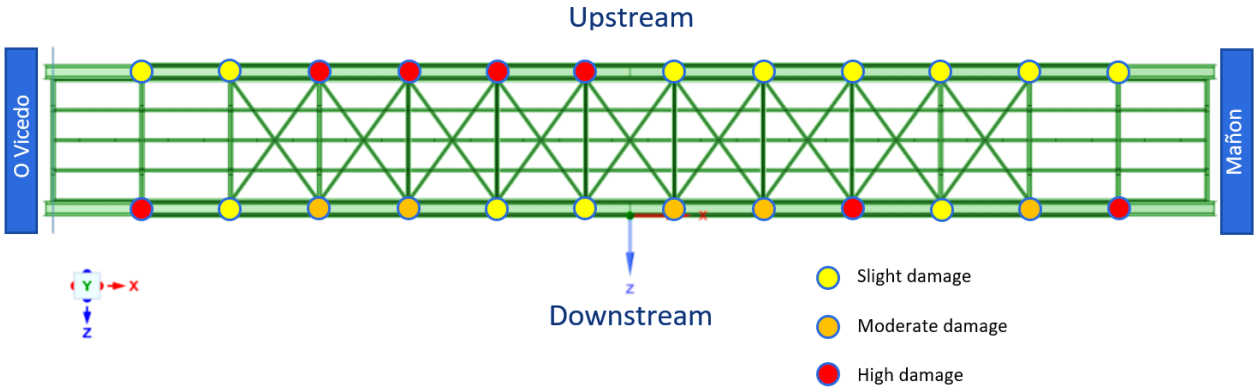


*Figure 3. Mapping of the damage state of the steel connections.*

With regards to the on-site (hand) measurements, a total of 325 values were obtained, spread over the main elements of the structure (arches, stringers, hangers, etc.), and on different regions (flange, web, etc.). The (rounded) mean values are summarized in Table 1.

| Element | Region | Thickness (mm) |
|---|---|---|
| Arch & Girder | Flange | 18 |
| | L-shaped profile | 11 |
| | Web | 24 |
| Hangers | Plate | 10 |
| | L-shaped profile | 8.5 |
| | Lacings | 10 |
| Stringers | Flange | 7 |
| | L-shaped profile | 8 |
| | Web | 8 |
| Transverse beams | Flange | 7 |
| | L-shaped profile | 11 |
| | Web | 10 |
| Lateral bracings | Height | 90 |
| | Width | 10 |
| Cross bracings | Radius | 10 |

*Table 1. Measures of the bridge elements as obtained from the experimental campaign.*

## 3.2 Terrestrial Laser Scanner

Recently, the use of geomatic approaches has experienced great development in the civil engineering field. In masonry bridges, for instance, photogrammetric approaches and Terrestrial Laser Scanner (TLS) have been postulated as a very useful tool for developing accurate numerical models with highly complex geometry [1].

TLS is usually the method of choice when the digitalization process entails difficult or dangerous access. Accordingly, in this work, a TLS survey was carried being the equipment employed the FARO Focus 3D x130. This equipment measures distances in a range of 0.6–120 m with an accuracy of ±2mm. The field of view is 305° vertically and 360° horizontally and its maximum angular resolution is 0.009°.

The 3D digitalization of the construction was performed through 10 scan positions. 4 of them were located under the deck and the remaining ones were on the deck. Exemplary, one of the under-deck scan positions is shown in Figure 4. The original point clouds had around 20 million points each. Once post-processed to filter noisy points and avoiding unwanted features (e.g. vegetation), the final point cloud was composed of 12.431.238 points.

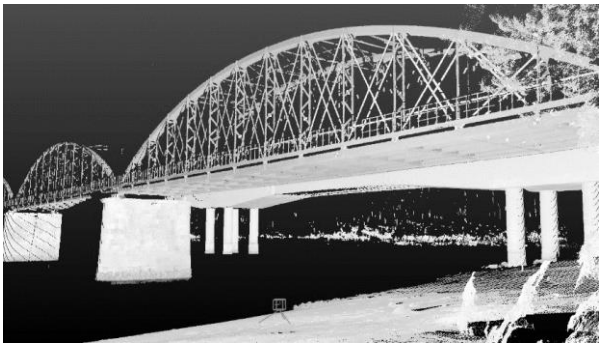

Figure 4. Example of a point cloud taken from the upstream side under the bridge deck.

### 3.3 Ambient vibration test

The experimental natural frequencies and mode shapes of the structure were obtained from a dynamical characterization campaign based on Operational Modal Analysis (OMA).

To design the most suitable setup for the test, a prior (simplified) numerical model was elaborated, and several simulations were performed. The first natural frequency was obtained around 1.00 Hz ($f_{\min}$) and the upper one around 10.00 Hz ($f_{\max}$). For this reason, the sampling frequency ($f_s$) was established at 128 Hz, following the criterion suggested in Ventura [2]; see Eq 1.

$$f_s > 2.4\, f_{\max} \qquad (1)$$

Regarding the acquisition time, different criteria can be found in the existing literature. L. F. Ramos states in [3] that if the structure is well excited, an acquisition time of 1000 times the highest natural period of interest is enough. Other authors such as J. Rodrigues [4] suggest using 2000 times the highest natural period of interest. In [2], the acquisition time is estimated following the criterion of Eq 2. In this work, since the structure was not well excited, the acquisition time was set to 45 min per setup, meeting all the aforementioned criteria.

$$T_{tot} > \frac{20}{2\varsigma f_{\min}} = \frac{10}{\varsigma f_{\min}} \qquad (2)$$

The equipment employed to perform the test were 6 uniaxial seismic accelerometers type 8340 with a sensitivity of 10V/g, and an acquisition module type 3050 with a frequency range of 0 - 51.2KHz, all of them of Brüel & Kjaer. Magnetic anchors joined to L-shaped steel supports were employed to fix the accelerometers to the structure. Due to the limited number of available sensors, a multi-setup test was considered. In figure 5 the measurement points are sketched. For each point, vibration measurements were taken in vertical and transversal directions. In the deck, the accelerometers were placed in the web girder, in the middle of each pair of hangers. As for the hanger points, they were placed on the inner side at a height of 3.00m.

The data obtained in the ambient vibration test were processed in the Artemis software using the SSI-PC algorithm [5]. As a result, 4 natural frequencies and their corresponding mode shapes were obtained. The first frequency is at 1.05 Hz and is a symmetrical transverse flexural mode of the whole bridge. The second natural frequency is at 2.71 Hz, and it is an antisymmetric flexural mode between the arch and the deck. The third natural frequency is at 6.19 Hz, and it is a vertical flexural mode of the whole structure. Finally, the fourth natural frequency is at 7.36 Hz, and it represents a torsional mode shape. The modes shapes are presented in Figure 6 and the natural frequencies are summarized in Table 2.

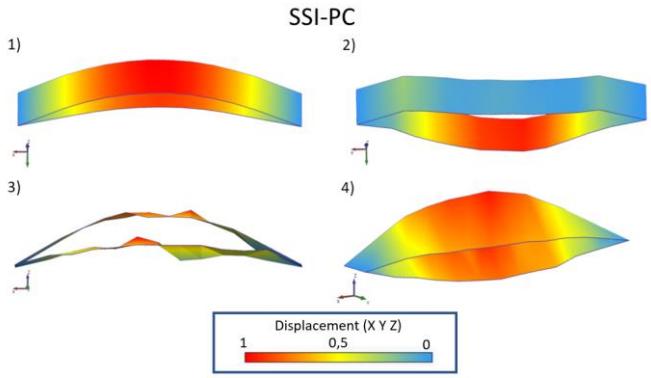


Figure 5. Experimental mode shapes as obtained from the ambient vibration test.

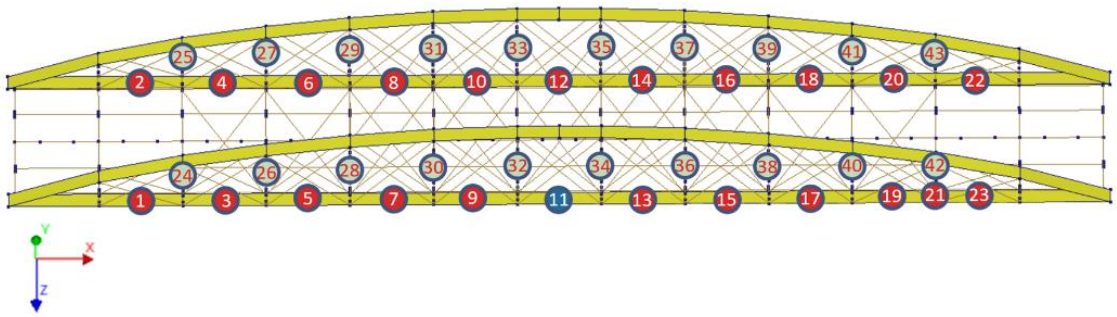


Figure 6. Accelerometer positions in the ambient vibration test.

| Experimental Modes | Frequency |
|---|---|
| Mode 1 | 1.05 Hz |
| Mode 2 | 2.71 Hz |
| Mode 3 | 6.19 Hz |
| Mode 4 | 7.36 Hz |

*Table 2. Natural frequencies as obtained from the ambient vibration test.*

## 4 Numerical model

A numerical model was developed following the Finite Element Method (FEM). The as-built geometry was extracted from the point cloud and the on-site measurements. The modeling process was performed using Diana FEA and MATLAB software packages. The mesh consisted mainly of first-order *Mindlin* beam elements, except for the arch and girder web, which were modeled using four-node quadrilateral isoparametric shell elements, and for the lateral and cross bracings which were modeled using two-node truss elements (see Figure 7).

The corrosion in some elements has resulted in a stiffness degradation of some of the steel connections. Thus, aimed at simulating its real semi-rigid behavior, several rotational springs were introduced between hangers and transverse beams. For the rest of the bridge, pinned and fully rigid connections were considered depending on the constructive scheme.

As for boundary conditions, translational springs in vertical (Y-axis) and transversal (Z-axis) directions were introduced at both supports. In the longitudinal direction (x-axis), displacements were fully restricted at one extremity and remaining free at the other. Finally, regarding the analysis procedure, a pre-stressed modal analysis considering dead loads was performed to account for the geometric nonlinearity (stress stiffening) of the lateral and cross bracings.

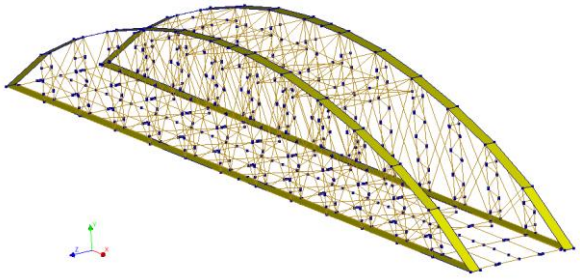

*Figure 7. Overall view of the FE Model of O Barqueiro bridge.*

## 5 Sensitivity analysis

To determine the most influential parameters on the natural frequencies and mode shapes of the bridge, a sensitivity analysis was carried out. This allows obtaining further insight into the mechanical response of the structure as well as reducing the computational cost of the subsequent optimization process. Initially, a total of 13 uncertain model inputs were considered, see Table 3.

| ID | Designation | Lower Bound | Upper Bound |
|---|---|---|---|
| V1 | Density | 7615 kg/m³ | 8085 kg/m³ |
| V2 | Young's modulus | 1.70E+11 N/m² | 2.32E+11 N/m² |
| V3 | Arches | -1.2 mm | 4.65 mm |
| V4 | Hangers | -1.1 mm | 4.65 mm |
| V5 | Stringers | -1 mm | 4.65 mm |
| V6 | Transverse beams | -0.95 mm | 4.65 mm |
| V7 | Reinforcement sheets | -1.9 mm | 4.65 mm |
| V8 | Rotational stiffness of low-damaged connections | 1.00E+05 Nm/rad | 1.00E+8 Nm/rad |
| V9 | Rotational stiffness of high-damaged connections | 1.00E+05 Nm/rad | 1.00E+8 Nm/rad |
| V10 | Translational stiffness of left support (Y-axis) | 1.00E+05 N/m | 1.00E+06 N/m |
| V11 | Translational stiffness of left support (Z-axis) | 1.00E+07 N/m | 1.00E+08 N/m |
| V12 | Translational stiffness of right support (Y-axis) | 1.00E+05 N/m | 1.00E+06 N/m |
| V13 | Translational stiffness of right support (Z-axis) | 1.00E+07 N/m | 1.00E+08 N/m |

*Table 3. Parameters considered in the model updating process.*

In the case of the material parameters, the lower and upper bounds were defined in accordance with the JCSS probabilistic model code [6]. For the density, these were derived by application of the three-sigma rule considering a Normal distribution with a mean of 7850 kg/m³ and a CoV (Coefficient of Variation) of 1% [6]. For Young's modulus, the boundaries were calculated using a confidence interval of 99.7% and assuming a lognormal distribution with a mean value of 200 N/mm² and a CoV of 5% [7,8].

Regarding corrosion effects and its impact on the geometric features of the steel members, it should be noted that at this stage of the research, a simplified approach was followed. Accordingly, a uniform loss of material was assumed for all affected elements, i.e., a uniform reduction of the cross-section dimensions. The lower bound of the thickness of the plates was derived by application of the procedure established in [9] and [10]. Thus, as the bridge is located in a coastal area, the annual corrosion was determined at 39 µm /year, obtaining a maximum thickness reduction of 4.65 mm. On the other hand, for the upper bound value, this was similarly established as the difference between the nominal thickness and the maximum measurement obtained in the experimental campaign. Finally, with regards to the stiffness of the rotational and translational springs, variation ranges were computationally derived from an extensive parametric analysis.

Sensitivity analysis was performed through the Pearson correlation coefficients:

$$\rho(X,Y) = \frac{cov(X,Y)}{[var(X)\ var\ (Y)]^{1/2}} \quad (3)$$

In this expression, $X$ represents any given model input and $Y$ a model response of interest. The Pearson correlation coefficients measure the degree of linear dependence, as well as is nature (positive or negative), between two random variables, adopting values in the interval [-1, 1]. Thus, a value close to one (or minus one) will indicate an exact positive (or negative) linear correlation.

The methodology was implemented using MATLAB software. To estimate the Pearson coefficients, a design of experiments of 750 samples was generated by Latin Hypercube Sampling (LHS) [11]. In Figure 8, the results of sensitivity analysis are summarized through the matrix of linear correlation coefficients between all model inputs (in blue) and output responses, i.e., frequencies and MAC values (in red). A threshold value of ± 0.2 was established to distinguish between influential and non-influential variables. The most influential are represented in red color while the less influential are represented in white. As it can be appreciated, the most important variables were: Young's modulus, the cross-section dimensions of the hangers, and the stiffness of the translational springs. These six model inputs will be considered in the subsequent updating process, while the rest of the variables were fixed at their nominal value.

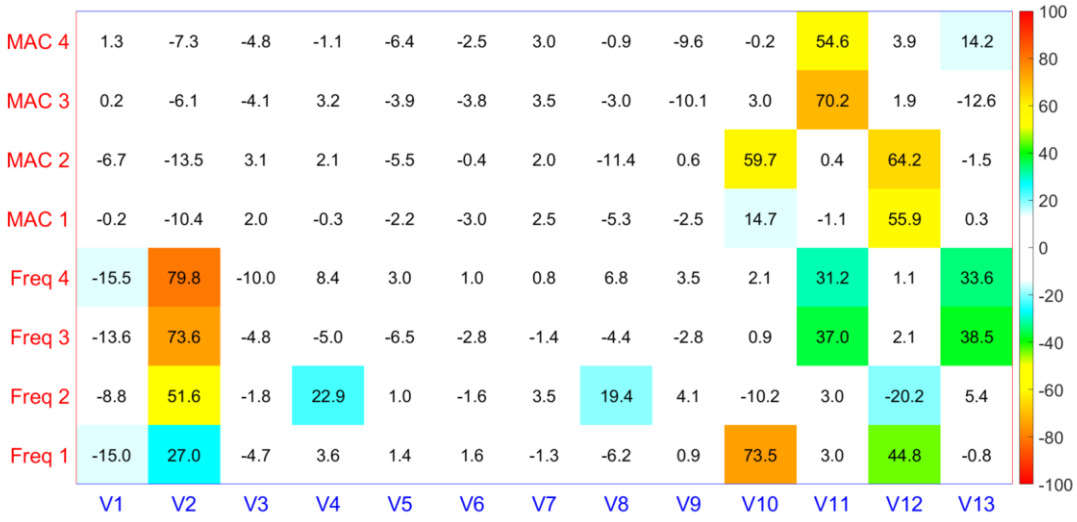


*Figure 8. Sensitivity analysis results based on Pearson correlation coefficients.*

## 6 Model updating

Once the most influential parameters were obtained, a deterministic model updating process was carried out. A non-linear least-squares formulation was adopted (Eq. 4), where $\pi(\boldsymbol{x})$ is the objective function to be minimized.

$$min_{\boldsymbol{x}}\|\pi(\boldsymbol{x})\|_2^2 = min_{\boldsymbol{x}} \sum_i \pi_i^2(\boldsymbol{x}) \qquad (4)$$

Numerical optimization is based on a trust-region-reflective algorithm, which determines a trust region to perform a second-order (quadratic) approximation *m(z)* of the objective function [12]. The approximation is defined by a truncated Taylor series of $\pi(\boldsymbol{x})$, being $\boldsymbol{x_s}$ the current state vector and $s$ the iteration number. The formulation is detailed in Eq. 5:

$$min_z\, m(\boldsymbol{z}) = \pi_s + [\nabla\pi_s]^T\boldsymbol{z} + \frac{1}{2}\boldsymbol{z}^T[\nabla^2\pi_s]\boldsymbol{z} \qquad (5)$$

being $\|\boldsymbol{z}\| \leq \nabla_s$

where $\boldsymbol{z}$ is the step vector from $\boldsymbol{x_s}$, $\pi_s$ is the value of the function, and $\nabla\pi_s$ and $\nabla^2\pi_s$ are the gradient and the Hessian of $\pi(\boldsymbol{x})$ at $\mathbf{x_s}$, respectively. The gradient and the Hessian are formulated as shown in Eq. 6 and 7. Herein, $J$ is the Jacobian, also called sensitivity matrix, and $\boldsymbol{r}$ is a vector of $k$ dimension containing the frequency and mode shape residuals.

$$\nabla\pi(\mathbf{x}) = J(\boldsymbol{x})^T r(\boldsymbol{x}) \qquad (6)$$

$$\nabla^2\pi(\mathbf{x}) = J(\boldsymbol{x})^T J(\boldsymbol{x}) + \sum_{i=1}^{k} \boldsymbol{r_i}(\boldsymbol{x})\nabla^2\boldsymbol{r_i}(\boldsymbol{x}) \cong J(\boldsymbol{x})^T J(\boldsymbol{x}) \qquad (7)$$

The methodology was implemented through the *lsqnonlin* function of the MATLAB optimization toolbox [13]. The objective function to be

minimized follows the formulation established in [14]:

$$\pi = \frac{1}{2}\left[W_f \sum_{i=1}^{m}\left(\frac{f_i^{num}-f_i^{exp}}{f_i^{exp}}\right)^2 + W_{MAC}\sum_{i=1}^{m}(1-MAC_i)^2\right] \quad (8)$$

where $f_i^{num}$ and $f_i^{exp}$ are the numerical and experimental frequencies, $MAC_i$ is the modal assurance criterion value between the numerical and experimental mode shape $i$, and $W_f$ and $W_{MAC}$ are the weighting factors of both terms, respectively. In this study, weights of 0.75 for $W_f$ and 0.25 for $W_{MAC}$ were adopted.

The calibrated parameter values are summarized in Table 4. The corresponding model outputs are indicated in Table 5 and they are compared with the values of the initial numerical model. Finally, the updated numerical mode shapes are depicted in Figure 9, where a strong similarity regarding the experimental mode shapes of the ambient vibration test can be observed. In general terms, a notable improvement was achieved, decreasing in more than 5% the mean total error and leading to an average frequency error of 2.09% and an average MAC of 0.97.

| Parameter | Value |
|---|---|
| V2 | 1.78 E+11 (N/m²) |
| V4 | -0.09375 (mm) |
| V10 | 4.27E+05(N/mm) |
| V11 | 4.7E+07(N/mm) |
| V12 | 4.34E+05 (N/mm) |
| V13 | 4.53E+07(N/mm) |

*Table 4. Model parameters after calibration.*

| Results | Exp. | Initial Model | Error (%) | Updated Model | Error (%) |
|---|---|---|---|---|---|
| F1 | 1.05 | 1.26 | 20.00 | 1.06 | 0.95 |
| F2 | 2.71 | 3.18 | 17.34 | 2.90 | 7.01 |
| F3 | 6.19 | 6.80 | 9.85 | 6.18 | 0.16 |
| F4 | 7.36 | 8.14 | 10.60 | 7.45 | 1.22 |
| MAC 1 | - | 0.99 | 1.00 | 0.99 | 1.00 |
| MAC 2 | - | 0.86 | 14.00 | 0.83 | 17.00 |
| MAC 3 | - | 0.95 | 5.00 | 0.95 | 5.00 |
| MAC 4 | - | 0.98 | 2.00 | 0.98 | 2.00 |

*Table 5. Model outputs and errors regarding experimental modal data of the initial and updated numerical model.*

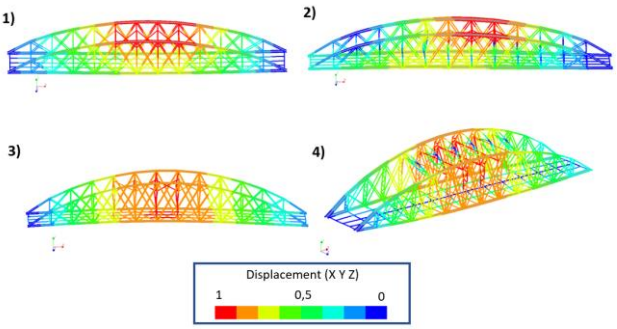


Figure 9. Numerical mode shapes after model calibration.

## 7 Conclusions

In this work, a multidisciplinary experimental campaign, FEM-based numerical modeling, and sensitivity analysis were carried out to perform a deterministic model updating of an ancient steel bridge. The results obtained present a high improvement regarding the original numerical model, decreasing the average total error from 9.97% to 4.29%. The main improvement was accomplished in the frequency error. The average frequency error was reduced of 14.45% to 2.34%.

The importance of an extensive and multidisciplinary experimental campaign is pointed out. Several sources of information are essential to building an accurate numerical model. Moreover, the key role of sensitivity analysis in the model updating process is highlighted. Sensitivity analysis helps not only to better understand and formulate the updating problem but also to reduce the computational cost by filtering non-influential variables.

Lastly, some possible improvements to the proposed workflow are underlined. Firstly, experimental tests to characterize the material properties of the bridge could be implemented to validate the results obtained in the model updating process. Secondly, other strategies of model calibration such as probabilistic or fuzzy approaches could be explored. This would allow comparing the agreement of the calibrated parameters values and even quantifying their

uncertainty in the form of posterior probability distributions.

## 8 Acknowledgments

This project has received funding from the European Union's Horizon 2020 research and innovation program under grant agreement No. 768171. This work has been partially supported by the Spanish Ministry of Science, Innovation, and Universities through the LASTING project Ref. RTI2018-095893-B-C21. This work has been partially supported by the Spanish Ministry of Science, Innovation, and Universities through the grant PRE2019-087331. This document reflects only the views of the authors. Neither the Innovation and Networks Executive Agency (INEA) nor the European Commission is in any way responsible for any use that may be made of the information it contains.

## 9 References

[1] Á. Bautista-De Castro, L. J. Sánchez-Aparicio, P. Carrasco-García, L. F. Ramos, and D. González-Aguilera, "A multidisciplinary approach to calibrating advanced numerical simulations of masonry arch bridges," *Mech. Syst. Signal Process.*, vol. 129, pp. 337–365, 2019, doi: 10.1016/j.ymssp.2019.04.043.

[2] C. E. V. Rune Brincker, *Introduction to operational modal analysis*. 2015.

[3] J. L. F. da S. Ramos, "Damage Identification on Masonry Structures Based on Vibration Signatures Identificação de Dano em Estruturas de Alvenaria Baseada na Medição de Vibrações," Universidade do Minho, 2007.

[4] J. Rodrigues, "Identificação Modal Estocástica: Métodos de Análise e Aplicações em Estruturas de Engenharia Civil," 2004.

[5] C. Rainieri and G. Fabbrocino, *Operational Modal Analysis of Civil Engineering Structures: An Introduction and Guide for Applications*. 2014.

[6] JCSS, "Probabilistic Model Code - Part 2: Load Models," *Jcss*, pp. 1–73, 2001.

[7] M. Barbato, A. M. Asce, Q. Gu, A. M. Asce, J. P. Conte, and M. Asce, "Probabilistic Push-Over Analysis of Structural and Soil-Structure Systems," no. November, pp. 1330–1341, 2010, doi: 10.1061/(ASCE)ST.1943-541X.0000231 CE.

[8] C. B. Park, R. D. Miller, and J. Xia, "Multichannel analysis of surface waves," *Geophysics*, vol. 64, no. 3, pp. 800–808, 1999, doi: 10.1190/1.1444590.

[9] AENOR Part 1: Corrosion of metals and alloys - Corrosivity of atmospheres - Classification and Corrosion, (ISO 9223:2012), *Documentos Europeos*. 2008, pp. 0–20.

[10] AENOR Part 2: Corrosion of metals and alloys - Corrosivity of atmospheres - Guiding values for the corrosivity categories and Corrosion, (ISO 9224:2012), *Documentos Europeos*. 2008, pp. 0–24.

[11] M. D. McKay, R. J. Beckman, and W. J. Conover, "Comparison of three methods for selecting values of input variables in the analysis of output from a computer code," *Technometrics*, vol. 21, no. 2, pp. 239–245, 1979, doi: 10.1080/00401706.1979.10489755.

[12] A. Teughels, J. Maeck, and G. De Roeck, "Damage assessment by FE model updating using damage functions," *Comput. Struct.*, vol. 80, no. 25, pp. 1869–1879, 2002, doi: 10.1016/S0045-7949(02)00217-1.

[13] Mathworks, "MathWorks. MatLab user manual,Least-Squares (Model Fitting) Algorithms."https://es.mathworks.com/help/optim/ug/least-squares-model-fitting-algorithms.html.

[14] Á. Bautista-De Castro, L. J. Sánchez-Aparicio, L. F. Ramos, J. Sena-Cruz, and D. González-Aguilera, "Integrating geomatic approaches, Operational Modal Analysis, advanced numerical and updating methods to evaluate the current safety conditions of the historical Bôco Bridge," *Constr. Build. Mater.*, vol. 158, pp. 961–984, 2018, doi: 10.1016/j.conbuildmat.2017.10.084.